Supplementary Materials for

Transcription under Torsion

Jie Ma, Lu Bai, and Michelle D. Wang

Correspondence to: mwang@physics.cornell.edu

This PDF file includes:

Materials and Methods

Supplementary Figures

Supplementary Movie

References

Materials and Methods

1. Protein and DNA preparations

E. coli RNAP, containing one hemagglutinin (HA) epitope tag on the C-terminus of each α-subunit, was purified by the method previously reported (*29*).

Three DNA templates were prepared for the single molecule experiments (Fig. S1). Two of them, termed "downstream" and "upstream", were used in either "downstream" or "upstream" stalling experiments. The "downstream" DNA template was also used in "transient torque pulse" experiments and "torque-velocity relationship" measurements. All three templates contained a main segment with a T7A1 promoter. This segment was amplified by PCR from a plasmid pLB601 (sequence available upon request) and digested with BsaI (37^0C, 1 hr) to generate a 4-bp 5'-overhang. The digested fragment was then ligated (16^0C, 4-6 hrs) to a short (56 bp) DNA segment containing a 6-biotin linker with biotin evenly spaced for attachment to a quartz cylinder (*8*) coated on one end with streptavidin. A third template, termed the "calibration" template, was used to calibrate the mechanical properties of the DNA in the absence of RNAP. Its method of preparation was similar to those we employed previously (*8-10*). The template was the same as the "downstream" template except that one end of the template was ligated to a 6-digoxigenin linker with dig tags evenly spaced for attachment to an anti-dig coated coverslip surface. All these DNA templates contain no known pause sites and their sequences are available upon request.

2. Angular optical trap

We have recently developed the angular optical trap (AOT), also termed the optical torque wrench (OTW), to enable direct torque and rotation detection of individual biological molecules (Fig. S2). For a review on this instrument, we refer the readers to our recent review (*30*). Below we will recap the basic features of our instrument based on this review. There are three core features of this instrument.

First, the trapping particle is a nanofabricated quartz cylinder, which has its extraordinary optical axis perpendicular to its cylinder axis and one of its ends chemically derivatized for attachment to a biological molecule of interest (*8*). Quartz has positive optical anisotropy, with a single axis more polarizable than the other two, so that a quartz particle is angularly confined by a linearly polarized light in two of its three Euler angles. The remaining Euler angle of the quartz cylinder is confined by the shape anisotropy intrinsic to an elongated cylinder. When a quartz cylinder is trapped by a linearly polarized laser, its cylinder axis aligns with the direction of light propagation so that the cylinder can be rotated about its axis by rotation of the laser polarization. Attaching a biological molecule specifically to one end of the cylinder allows the application of force to the molecule along the laser propagation direction, permitting independent control of force and torque. Nanofabrication techniques allow for the mass production of cylinders of uniform size, shape, and optical properties, as well as specific chemical derivatization of only one end of each cylinder. The cylinders may be fabricated using optical

lithography (*8*) or, for more selective localization of a molecule's attachment point, by electron-beam lithography (*31*).

The second feature of an AOT is a rapid and flexible control of the input linear polarization of the trapping laser beam, so that the instrument may function in different modes of operation (*7*). The use of a pair of acousto-optic modulators (AOMs) provides continuous and rapid control (~ 100 kHz) of the input polarization (*7*).

Finally, torque detection in an AOT is based on the change in the ellipticity of the trapping beam after it interacts with the trapping particle, a method independently demonstrated by two different groups (*7, 32*). In an AOT, a quartz cylinder is trapped such that its extraordinary axis, which is more polarizable than the other two axes, is aligned with the input beam's linear polarization. If the cylinder is rotated away from this stable trapping orientation, there will be a restoring torque, which arises due to misalignment of the particle's polarization and the electric field. Direct torque measurements are subsequently made by measuring the change in the angular momentum of the transmitted beam downstream of the trapped particle, which is accomplished by splitting the beam into its left- and right-circular components and determining their differential intensities (*7, 32*).

In an AOT, the same trapping beam is used for both torque and angle detection of the trapped particle, without the need for a secondary detection beam or imaging method. Such a detection method is exceedingly direct, relying solely on conservation of angular

momentum. During a typical experiment, force, displacement, torque, and angle of the cylinder are simultaneously measured at kilohertz frequencies, making this method well suited for the study of fast events.

3. Single molecule assays

Paused transcription complexes (PTCs) were formed prior to the single molecule experiments following protocols similar to those previously described (*16, 29, 33, 34*). Briefly, 25 nM *E. coli* RNAP was incubated with 5 nM DNA templates (either "downstream" or "upstream"), 250 μM ApU (initiating dinucleotide), and 50 uM ATP/CTP/GTP in the "transcription buffer" (25 mM Tris–HCl, pH 8.0,100 mM KCl, 4 mM $MgCl_2$, 1 mM DTT, 3% (v/v) glycerol) at 37^0C for 30 mins. The resulting PTCs contained transcription elongation complexes paused after synthesizing 20 nt nascent RNA due to the lack of UTPs in the buffer.

The single molecule experiments described in the main text were then carried out in an environmentally controlled room at 23.2 ± 0.5 ^{0}C. During an experiment, RNAPs from these PTCs were torsionally constrained to a coverslip surface coated with anti-HA antibodies through two HA/anti-HA interactions. Depending on the experiment, either the downstream or upstream end of the DNA was torsionally constrained to the bottom of a nanofabricated quartz cylinder via multiple biotin/streptavidin linkages (Fig. 1A). Transcription was resumed by the addition of the transcription buffer supplemented by 1

mM NTPs, and 2.5 mM protocatechuic acid (PCA) and 20 nM protocatechuate-3,4-dioxygenase (PCD) to reduce photo-damage (*35*). During an experiment, the cylinder was held in a laser trap of 10-15 mW at the trap center. This low laser power introduced minimal heating at the specimen plane. We estimate (*36*) that the temperature at the RNAP during a measurement to be about 23.3 ± 0.5 ^{0}C.

4. Data collection and analysis

Experimental data were low-pass filtered to 1 kHz, digitized at 2 kHz, and further averaged to 200 Hz. To determine the RNAP stalling torque, the force at which RNAP was stalled was converted into torque using the pre-calibrated torque-force relationship from DNA winding experiments (Fig. S3). The method of conversion to transcript size can be found in the section entitled "Conversion of data to RNAP position on DNA template". Although the presence of a plectoneme greatly amplified the extension in the detection of RNAP movement and thus enhanced the measurement's sensitivity, noise due to the low force used in the experiments and instrument drift only permitted detection of backtracking in traces that exhibited reverse translocation of several bp over a few seconds as shown in Figure 2C.

The transcription rate at a constant torque was obtained from the slope of DNA extension versus time in the region of traces where DNA remained buckled and the DNA extension was at least 250 nm. Instantaneous velocity at each data point of a trace was calculated

after Gaussian filtering the data to 10 Hz. An instantaneous velocity distribution was then generated by weighting each template position equally (*29, 34*) and a mean velocity was computed from this distribution. The instrument drift was ~0.8 nm/s along *z* and its contribution to the velocity calculation was negligible when DNA was buckled. For pause analysis, we followed a previously developed algorithm (*29, 34*) to detect pauses from a plot of dwell time vs. filtered (10 Hz) transcript position. The cutoff duration was set to be 0.2 s (i.e., an RNAP was considered to have paused if the time it spent at a single nucleotide position was greater than 0.2 s). The 0.2 s was found to be 4 times the most likely dwell time which represented the baseline.

For the zero torque condition (Fig. S8), because DNA was not torsionally-constrained, the experimental configuration was similar to those previously reported (*29, 34*) except that a very low resisting force (0.3 pN) was applied along the *z* direction. The lower sensitivity of these experiments required drift correction of the velocity and more substantial Gaussian filtering (0.67 Hz instead of 10 Hz). Such filtering precluded detection of short pauses (0.2-2 s) and thus the zero-torque traces were not used for pause analysis.

5. DNA supercoiling characterization

In order to extract desired information (such as stall torque, RNAP template position, transcription velocity, etc.) from measured data (such as force, DNA extension, etc.), we

had to first characterize DNA supercoiling properties of either (+) or (–) supercoiled DNA, following methods previously described (*9, 10*). Experiments were conducted using the "calibration" DNA template in the transcription buffer. Figure S3 shows measured DNA extension and torque traces during DNA supercoiling, as well as the extension change per turn ($\Delta z_{\text{perturn}}$), and the torque (τ) after either DNA buckling or DNA melting as a function of force.

B-DNA

Prior to buckling or melting, DNA remains in a B-form during supercoiling. Its extension and torque have been well studied previously (*9 , 37*).

DNA extension is well described by theoretical work by J.F. Marko (*9, 37*):

$$\frac{z}{L} = 1 - \frac{1}{2}\sqrt{\frac{k_{\text{B}}T}{L_{\text{p}}F}} - \frac{{\omega_0}^2 C^2}{16}\left(\frac{k_{\text{B}}T}{L_{\text{p}}F}\right)^{\frac{3}{2}}\sigma^2, \qquad (1)$$

where L is the DNA contour length, $k_{\text{B}}T$ is the thermal energy, F is the applied force, L_{p} is DNA bending persistence length, $\omega_0 \equiv 2\pi\varpi_0 = (2\pi/3.57)nm^{-1}$, and σ is the specific linking number.

DNA also behaves like a linear torsional spring under twist, with a force-dependent torsional spring constant. Torque is simply proportional to twist angle or specific linking number:

$$\tau = k_B T \omega_0 C_s \sigma \,, \tag{2}$$

and

$$C_s = C\left(1 - \frac{C}{2}\sqrt{\frac{k_B T}{4L_p^3 F}}\right), \tag{3}$$

where C is the intrinsic twist persistence length of DNA and C_s is the twist persistence length of the extended state under force.

Under our experimental conditions, we measured that L_p = 43 nm and C =100 nm, and $k_B T$ = 4.08 pN•nm.

DNA melting

Once DNA started to melt, the melting torque was insensitive to the force and averaged to ~11 pN·nm under our experimental conditions (Fig. S3). This property has also been previously shown to have minimal dependence on the DNA length over the range of length relevant to this study (*9, 10*).

In the past two decades, a number of single molecule studies have investigated the DNA melting transition. The initial indication of the melting transition upon under-winding came from the seminal work by Strick and colleagues (*38*) who twisted DNA under a constant force using magnetic tweezers. They found that the extension signal became asymmetric about zero turns added when the force was increased above 0.5 pN.

Subsequently, John F. Marko formulated a theoretical framework and predicted that melting transition takes place approximately −10 pN·nm (*37, 39*). More direct evidence for the melting transition was only obtained after the advent of experimental techniques capable of direct torque detection. During a phase transition, torque plateaus and thus serves as an excellent indicator of the transition. Bryant et al. (*40*), using a rotary bead assay, first directly measured the melting torque to be approximately −11 pN·nm. This value was further supported by subsequent measurements from both our lab (*10*) and several other groups (*41-43*). A more detailed discussion on this topic can be found in our recent review article in the Annual Review of Biophysics (*30*).

The melting torque value measured for this work is in accord with those of previous measurements and theoretical work. During DNA under-winding, DNA is expected to buckle before DNA melting under a force < 0.5 pN, and to melt first under a force ≥ 0.5 pN. Figures S3A and S3B show measured extension and torque versus number of turns added under a constant force. Indeed, under a force < 0.5 pN, the measured extension decreased symmetrically about zero turns, and the torque plateaued upon DNA buckling with the torque magnitude being the same for both over- and under-winding. Under a force ≥ 0.5 pN, the measured over-winding buckling torque continued to increase with an increase in force, while the under-winding torque plateau remained at approximately −11 pN·nm. The torque plateau around −11 pN·nm, as well as the extension asymmetry, has been viewed as the signature of the melting transition (*10, 40, 42, 43*).

Melting torque is also expected to be sequence-dependent. In our studies, DNA templates

lacked any long stretches of AT or GC rich regions and we found that the torque signal was rather flat during the melting transition, hovering around −11 pN·nm ((*10*), Fig. S3). It is possible that there are small sequence-dependent effects that were masked by the measurement uncertainty (~ ±1 pN·nm). Other groups that used random DNA sequences have also reported similar flat torque plateaus during melting (*40, 42*). Recently, Oberstrass et al. (*43*) specifically investigated sequence-dependent DNA melting. They found that a long GC repeat stretch that favors Z-DNA formation underwent a transition to Z-DNA at −3 pN·nm. Although they did not examine AT rich tracks, they found that mismatch bubbles underwent a structural transition at a torque of −5 pN·nm. This suggests that an AT rich track will likely melt at a torque intermediate between −11 and −5 pN·nm. Their subsequent experiments indeed confirmed this speculation (*44*). They found the melting torque for AT rich regions to be ~ −7.5 pN·nm.

DNA extension after melting has been experimentally investigated previously (*45, 46*). These studies show that extension decreases rather linearly with under-winding. Figure S3C shows how the DNA extension change per turn depends on force.

DNA buckling

DNA supercoiling behavior has been previously described theoretically by John F. Marko (*37*). The Marko model predicts the following relation for the post-buckling torque:

$$\tau_{\mathrm{b}} = \sqrt{\frac{2k_{\mathrm{B}}TPg}{1-P/C_{\mathrm{s}}}} = \sqrt{\frac{2k_{\mathrm{B}}TP\left(F-\sqrt{\frac{k_{\mathrm{B}}TF}{L_{\mathrm{p}}}}\right)}{1-\frac{P}{C}\cdot\frac{1}{1-\frac{C}{2}\sqrt{\frac{k_{\mathrm{B}}T}{4L_{\mathrm{p}}^{3}F}}}}}, \quad (4)$$

where g is the free energy of stretched DNA per unit length under no torsional constraints:

$$g = F - \sqrt{\frac{k_{\mathrm{B}}TF}{L_{\mathrm{p}}}} \quad (5)$$

We thus fit our measured torque-force relationship with Eq. 4 with the only fitting parameter being P (Fig. S3D). The best fit yielded $P = 27$ nm.

Figure S3C shows how the DNA extension change per turn after buckling depends on force. Our measured DNA extension is in agreement with those previously established (*9, 13, 47*). All these studies show that extension decreases rather linearly with over-winding. Although the Marko model provides a good fit tor torque, it does not fit well for extension per turn after buckling or melting for the range of force shown in Fig. S3C.

Our angular optical trap directly measures torque but requires averaging to achieve accurate torque values. This is not always compatible with dynamic measurements. On the other hand, force can be measured accurately with significantly less averaging. Because there is a well-defined relation between torque and force during DNA supercoiling (Fig. S3), force can serve as a faster and more accurate indicator of torque, and this feature was exploited in this work during transcription measurements.

6. Conversion of data to RNAP position on DNA template

In order to determine RNAP position on the DNA template in real time, the DNA contour length, $L(t)$, between the RNAP and the cylinder must be determined from measured quantities (force, extension, and number of turns mechanically introduced). Once the DNA elastic parameters are determined, DNA contour length is solely determined by extension, force, and linking number (or linking number density).

In the first part of this section, we use an example data trace from the downstream stalling experiments (Fig. 1B) to illustrate the details of this data conversion. In this type of experiment, after 1mM NTPs were introduced into the sample chamber, quite often RNAP had already (+) supercoiled DNA before the cylinder was trapped. Therefore, a preparation step (referred to as step 0) was used to quickly unwind DNA to convert it into (–) buckled states under a constant low force. After this step, the cylinder angle was held fixed. At steps 1-3, RNAP transcribed under a constant low force. During these steps, RNAP transcription converted DNA from a (–) plectoneme state (step 1), to a non-plectoneme state (step 2), and then to a (+) plectoneme state (step 3). At step 4, the force clamp was turned off and RNAP was allowed to build up torque until it finally reached a stall. Since extension changes in steps 1-4 were solely due to transcription, we focus the following discussion on these steps.

In order to convert measurements to RNAP template position, we make the following assumptions. (1) RNAP helically tracks along the helical groove of the DNA template

during elongation as well as during backtracking, because of the groove-tracking nature of RNAP (*12, 48*). (2) Changing the tension on a template with a plectoneme affects RNAP only via changes in DNA torque, and not via specific effects of plectonemes.

We denote the total linking number at the end of step 0 as Lk_s. During steps 1-4, because the angle of the cylinder was fixed and RNAP was torsionally constrained to the coverslip, the linking number was conserved, i.e.,

$$Lk(t) = Lk_s \tag{6}$$

However, the linking number density, $\sigma(t)$, increased with time due to the shortening of the DNA contour length, L, between the polymerase and the cylinder:

$$\sigma(t) = \frac{Lk(t) - Lk_0(t)}{Lk_0(t)} = \frac{Lk_s - Lk_0(t)}{Lk_0(t)} = \frac{Lk_s - L(t)\varpi_0}{L(t)\varpi_0} = \frac{l}{L(t)} - 1, \tag{7}$$

Where Lk_0 is the linking number of the relaxed DNA, $l \equiv Lk_s / \varpi_0$, and $\varpi_0 = (1/3.57)\text{nm}^{-1}$ is an inverse of the helical repeat. Therefore,

$$L(t) = \frac{l}{1 + \sigma(t)} \tag{8}$$

Our overall strategy in obtaining $L(t)$ is divided into three stages of data conversion. i) Determine Lk_s from the measured extension maxima, z_{max}, at step 2. ii) Convert the extension measured during steps 1-3 to DNA contour length. iii) Convert the measured extension data during step 4 to DNA contour length.

i) Determine Lk_s from the measured extension maxima, z_{max}, at step 2.

Based on theoretical work by J.F. Marko (*37*), before DNA is buckled, the extension *z* is given by

$$\frac{z(t)}{L(t)} = 1 - \frac{1}{2}\sqrt{\frac{k_B T}{L_p F}} - \frac{\omega_0^2 C^2}{16}\left(\frac{k_B T}{L_p F}\right)^{\frac{3}{2}}\sigma(t)^2 = a + b\sigma(t)^2, \quad (9)$$

where $\omega_0 \equiv 2\pi\varpi_0 = (2\pi/3.57)\,\mathrm{nm}^{-1}$, $a \equiv 1 - \frac{1}{2}\sqrt{\frac{k_B T}{L_p F}}$, and $b \equiv -\frac{\omega_0^2 C^2}{16}\left(\frac{k_B T}{L_p F}\right)^{\frac{3}{2}}$. Notice that $a > 0$, $b < 0$, and $|a| << |b|$.

Substituting Eq. 8 into 9 yields

$$z(t) = \frac{l}{1+\sigma(t)}(a + b\sigma(t)^2) \quad (10)$$

Eq. 10 can then be used to determine σ_0, at which extension *z* reaches a maximum by setting $dz/d\sigma = 0$ and solving for σ_0:

$$\sigma_0 = -1 + \sqrt{1 + \frac{a}{b}} \approx \frac{a}{2b}, \text{ as } |a| << |b|. \quad (11)$$

Thus

$$z_{max} = \frac{l}{1 + a/2b}(a + a^2/4b). \quad (12)$$

Finally,

$$Lk_s = l\varpi_0 = \frac{z_{max}\varpi_0}{a(1 + a/4b)}(1 + a/2b) \quad (13)$$

This equation shows how Lk_s can be determined from the measured z_{max}.

ii) Convert the extension measured during steps 1-3 to DNA contour length.

Using the calculated Lk_s together with Eqs. 6 and 8, we have

$$\frac{z(t)}{L(t)} = a + b\sigma(t)^2 = 1 - \frac{1}{2}\sqrt{\frac{k_B T}{L_p F}} - \frac{\omega_0^2 C^2}{16}\left(\frac{k_B T}{L_p F}\right)^{\frac{3}{2}}\left(\frac{Lk_s/\varpi_0}{L(t)} - 1\right)^2. \quad (14)$$

Given the measured extension $z(t)$, Eq. 14 is a quadratic equation in $L(t)$ and can be solved for $L(t)$. Subsequently $\sigma(t)$ can also be calculated using Eq. 7.

The linking number density, DNA contour length, and extension at the boundary of steps 1 and 2 are given by the following expressions (*37*):

$$\sigma(t_{1\to 2}) = -\sigma_s = -\frac{1}{c_s}\left(\frac{2pg}{1 - p/c_s}\right)^{1/2} \quad (15)$$

$$L(t_{1\to 2}) = \frac{l}{1 + \sigma(t_{1\to 2})} = \frac{l}{1 - \sigma_s} \equiv L_a \quad (16)$$

$$z(t_{1\to 2}) \equiv z_a \quad (17)$$

where $p \equiv k_B T P \omega_0^2$, $c_s \equiv c\left(1 - \frac{C}{4L_p}\sqrt{\frac{k_B T}{L_p F}}\right)$, and $c \equiv k_B T C \omega_0^2$.

Similarly, at the boundary of step 2 and 3, we have

$$\sigma(t_{2\to 3}) = \sigma_s = \frac{1}{c_s}\left(\frac{2pg}{1 - p/c_s}\right)^{1/2} \quad (18)$$

$$L(t_{2\to 3}) = \frac{l}{1 + \sigma(t_{2\to 3})} = \frac{l}{1 + \sigma_s} \equiv L_b \quad (19)$$

$$z(t_{2\to 3}) \equiv z_{\mathrm{b}}. \tag{20}$$

For steps 1 and 3 where DNA remained buckled, we wish to verify that the extension change Δz was proportional to DNA contour length change ΔL which corresponds to the distance RNAP translocated:

$$\Delta z = \mp \alpha \Delta L \tag{21}$$

α is a constant which only depends on force, and the $\mp$ correspond to steps 1 and 3 respectively.

We will first consider step 3. Because the extension has a linear relation with turns (Fig. S3), we assume that the extension goes to zero at the end of a fully buckled state, similar to treatment in the Marko model (*37*),

$$\frac{z}{L} = \frac{\sigma_{\mathrm{p}} - \sigma}{\sigma_{\mathrm{p}} - \sigma_{\mathrm{s}}} \frac{z(\sigma_{\mathrm{s}})}{L} = A_{\mathrm{s}} + (\sigma - \sigma_{\mathrm{s}})k, \tag{22}$$

where $A_{\mathrm{s}} \equiv \frac{z(\sigma_{\mathrm{s}})}{L}$ and $k \equiv -\frac{A_{\mathrm{s}}}{\sigma_{\mathrm{p}} - \sigma_{\mathrm{s}}}$, both of which are only dependent on *F*. Therefore

$$\frac{dz}{dL} = A_{\mathrm{s}} - k\sigma_{\mathrm{s}} - k = -k(1 + \sigma_{\mathrm{p}}) = \alpha. \tag{23}$$

The physical meaning of α is illustrated by Fig. S9. $(A_{\mathrm{s}} - k\sigma_{\mathrm{s}})$ is the vertical axis intercept of the straight line extrapolated from the plectoneme region and k is the slope of the curve. Since $(A_{\mathrm{s}} - k\sigma_{\mathrm{s}}) \sim 1 << |k|$ under low force conditions, α is dominated by k.

Therefore for step 1,

$$L(t) = L_a + \Delta L(t) = L_a + (z_a - z(t))/\alpha \tag{24}$$

and for step 3,

$$L(t) = L_b - \Delta L(t) = L_b - (z_b - z(t))/\alpha \tag{25}$$

Under the experimental conditions used here, for example, F = 0.3 pN, $\alpha \sim 15$. Therefore, for each base pair transcribed, there is a corresponding extension change of ~ 5 nm. This demonstrates that the presence of a plectoneme greatly amplified the RNAP movement, so that the DNA extension was exceedingly sensitive to transcription.

iii) Convert the measured extension data during step 4 to DNA contour length.

During step 4, because force/torque varies with time, the data conversion becomes more complicated. As with steps 1-3, the linking number is still conserved: $Lk = Lk_s$. Following Eq. 22,

$$\frac{z}{L} = \frac{\sigma_p - \sigma}{\sigma_p - \sigma_s}\frac{z(\sigma_s)}{L} = \frac{\sigma_p - \dfrac{Lk_s - L\varpi_0}{L\varpi_0}}{\sigma_p - \sigma_s} A_s, \tag{26}$$

where σ_p, σ_s, and A_s are solely functions of force and are known once the force is measured. Thus,

$$L(t) = \frac{\dfrac{z(t)\cdot(\sigma_p - \sigma_s)}{A_s} + \dfrac{Lk_s}{\varpi_0}}{1 + \sigma_p} = \frac{z(t) - kl}{\alpha}, \tag{27}$$

where k and α are only functions of force. Since force is measured directly, Eq. 27 thus determines the DNA contour length over time. In addition, we numerically calculated F versus L, given the twist, DNA contour length, force, and trap stiffness at the beginning of step 4 (which are all known after data conversion in step 3). We found that F is rather linear with L over the range of stall force (Fig. S11). Thus, a force change serves as a convenient indicator for transcription rate.

We can use a similar method to convert data in "upstream" stall torque experiments into RNAP position on the DNA template. One example is shown in Fig. S4. The conversion procedures are identical to those of the downstream case for steps 1-3. For step 4, they are also identical if the RNAP was stalled prior to DNA melting. Once DNA melting starts ($F \geq 0.5$ pN), the conversion procedures are also similar to those of the downstream case except that σ_p for the buckled state in Eqs. 26-27 needs to be replaced by σ_{m}, an effective specific linking number that allows the extension of the melted state to be expressed in a similar form as that of Eq. 22. Again, we numerically calculated F versus L (Fig. S11) and found that, in comparison to downstream stalling, force is less sensitive to RNAP translocation due to lower extension sensitivity to added twist upon DNA melting (Fig. S3C). The sensitivity also decreases with an increase in force. At 0.75 pN (the maximum force for upstream stalling), the force sensitivity $\frac{dF}{dL}$ is 1/3 of that of the corresponding downstream stalling. Nonetheless, this lowered sensitivity is still sufficient for the detection of stalling. We thus conclude that the observed force plateau in each upstream trace was due to RNAP stalling and not a result of a loss of detection

sensitivity.

This conversion procedure also allows the determination of torque as a function of time during a stalling experiment. The conversion steps are summarized below:

Steps 2 (pre-buckling/melting):

- Find Lk_s using Eq. 13.
- Find $\sigma(t)$ using Eq. 10. Alternatively, find $L(t)$ from Eq. 14 and then find $\sigma(t)$ using Eq. 7.
- Find $\tau(t)$ using Eq. 2.

Steps 1, 3, and 4 (post-buckling/melting):

- Find $\tau(t)$ using measured force $F(t)$ and calibration data in Fig. S3D.

7. Torque partition and torque relation with force.

Torque partition

The twin-supercoiled domain model suggests that both (−) supercoiling upstream and (+) supercoiling downstream generate a resisting torque on RNAP (*1*). This can be understood from an energetic point of view. In order for RNAP to move forward on the

template, RNAP must simultaneously unwind the downstream DNA and rewind the upstream DNA to maintain the transcription bubble. When RNAP works against (+) supercoiling downstream, torque resists unwinding of the downstream DNA to propagate the transcription bubble. Similarly, when RNAP works against (−) supercoiling upstream, torque resists rewinding of the upstream DNA to propagate the transcription bubble. Therefore, torque regulates elongation rates by regulating the energetics of the transcription elongation complex.

The current work focuses on stall torque measurements in which a resisting torque is present either upstream or downstream. In the twin-supercoiled domain model, both upstream and downstream DNA domains are closed (i.e., torsionally anchored), so that a resisting torque is generated by both (−) supercoiling upstream and (+) supercoiling downstream. In that case, the stalling torque will be partitioned between the upstream and downstream DNA domains. Based on energetic considerations, we expect that RNAP will stall when the sum of the total resisting torque from upstream and downstream reaches its stall torque. *In vivo*, the exact torque partitioning depends on the relative size of the two domains with the smaller domain accumulating more specific linking number during transcription. If the upstream domain is much smaller than the downstream DNA, then RNAP can still generate sufficient torque to melt upstream DNA; otherwise, RNAP may not melt upstream DNA or may only melt DNA sequences that are prone to melting at torques smaller than −11 pN·nm. In addition, the exact torque partition also depends on the actions of topoisomerases which preferentially

relax/generate (−) supercoiling or relax (+) supercoiling, likely leading to an asymmetric torque buildup.

(−) or (+) supercoiling may serve either an assisting or resisting role for transcription, depending on the location of supercoiling relative to the RNAP (Fig. S10). (−) supercoiling resists transcription when located upstream but facilitates transcription when located downstream. Conversely, (+) supercoiling facilitates transcription when located upstream but resists transcription when located downstream.

Torque relation with force

Because of the helical structure of double-stranded DNA, during transcription elongation RNAP must simultaneously translocate along DNA and rotate around it. Therefore, RNAP may need to work under both an external force (F) and an external torque (τ). Based on purely energetics considerations, a force can be converted to an equivalent torque, and vice versa, via the following relationship (*49*): $Fd = \tau\theta$, where d represents the contour length of DNA per bp (~0.34 nm), and θ represents the angular rotation of RNAP after 1 bp translocation (0.60 radian or ~34°, converted from 10.5 bp per turn). Previously, the stall force of *E. coli* RNAP has been measured to be ~ 25 pN (*50, 51*). This corresponds to a stall torque of ~ 14 pN·nm, comparable, but slightly higher than, our measured torque of 11 pN·nm. This discrepancy may indicate that force and torque may induce different conformational changes in the elongation complex, introducing new energy terms that are not taken into account by the energetic conversion $Fd = \tau\theta$.

RNAP may be stalled solely by torque, by force, or by a combination of the two. Note that for all experiments in the current work, a small force (< 1.5 pN) was applied to the RNAP in addition to torque. Since this force is much smaller than the stall force of ~ 25 pN, RNAP was stalled under essentially only the influence of torque with minimal contribution from force.

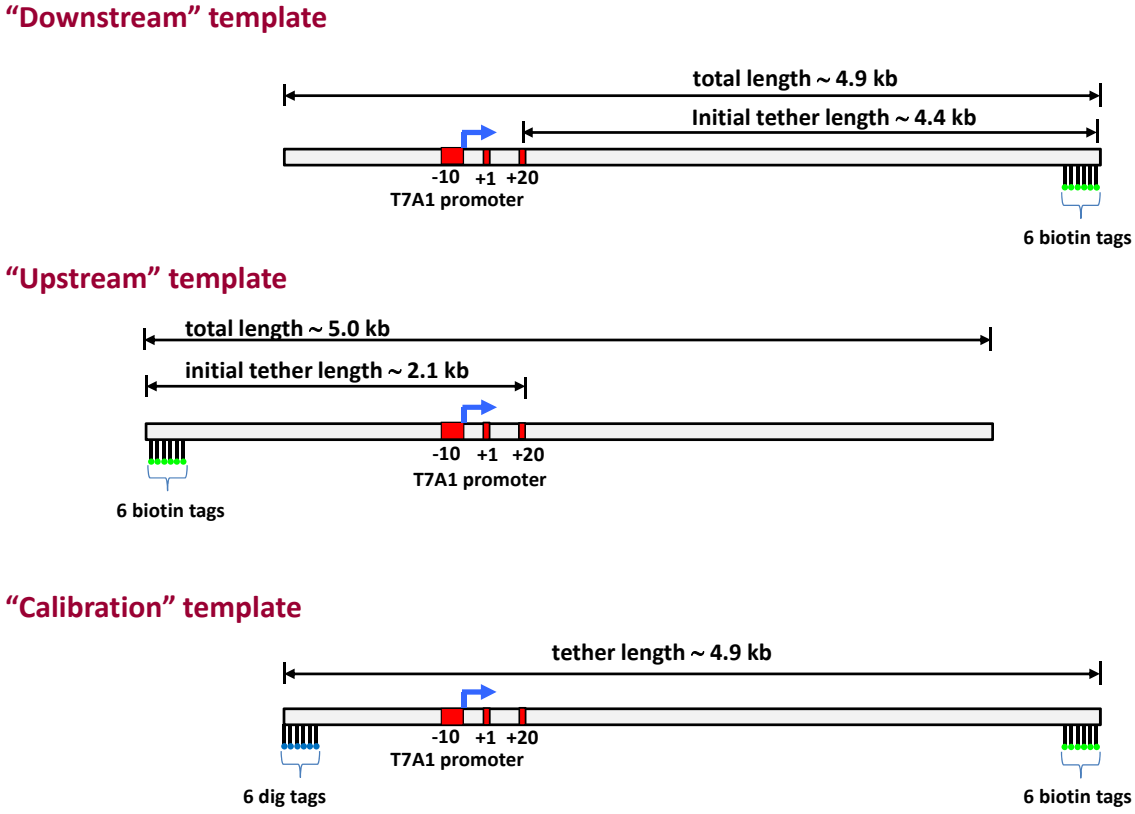

Figure S1. Single molecule DNA templates.

"Downstream" template was used in experiments on downstream stalling, torque jump, and torque-velocity. "Upstream" template was used in "upstream stalling" experiments. The "calibration template" was used to characterize DNA supercoiling properties.

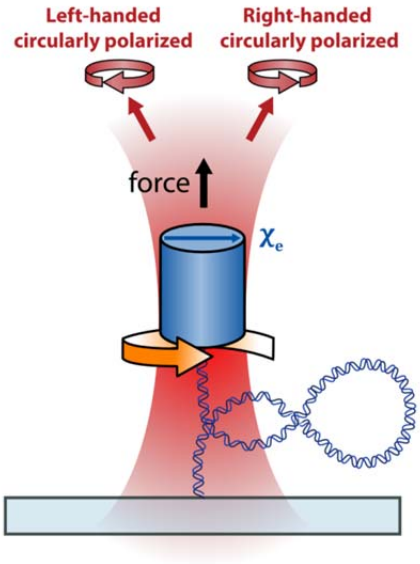

Figure S2. Experimental configuration for using an angular optical trap (AOT) to study DNA supercoiling. The angular optical trap angularly orients a quartz cylinder using the linear polarization of the input trapping laser beam. The polarization state of the transmitted beam, as measured by the transmitted light intensities in the right and left-handed circular polarizations, directly determines the applied torque on a dsDNA molecule and the angular orientation of the DNA end.

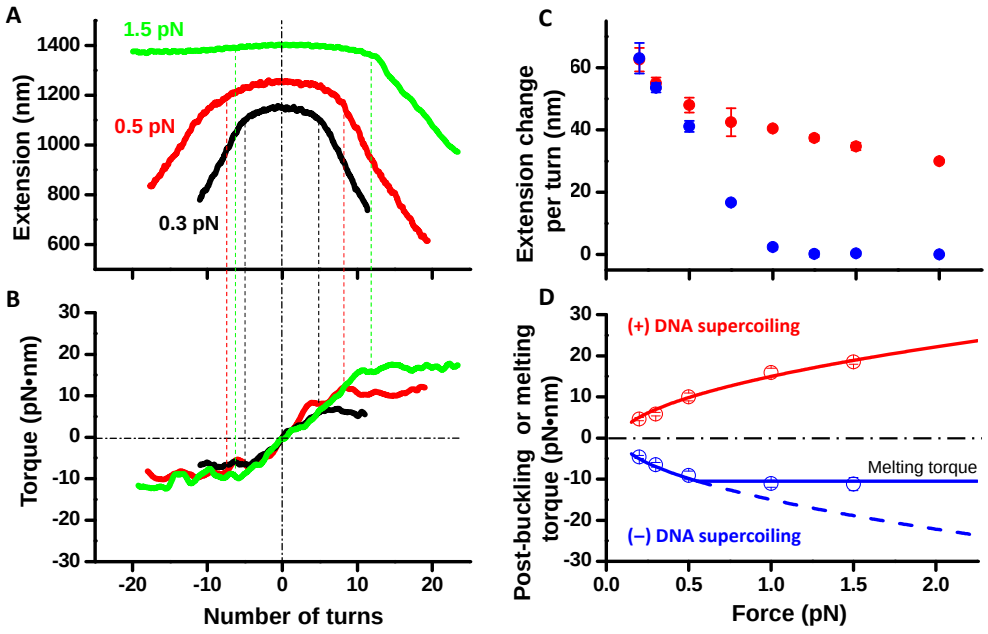

Figure S3. Characterization of extension and torque during DNA supercoiling.

Following previously described methods (*9*, *10*), we supercoiled DNA under a constant force. (**A**) and (**B**) are examples of the measured extension and torque of DNA, respectively. Here we define torque to be (+) when DNA was over-wound and (–) when it was under-wound. We then characterized (**C**) extension per turn and (**D**) torque after DNA was buckled or melted during DNA supercoiling. Briefly, the measurements were carried out using the "calibration" template in the transcription buffer. DNA was held under a constant force while twist was added to DNA. The torque in the DNA increased while the extension decreased slightly, until DNA buckled to form a plectoneme or melt. Upon plectoneme formation, torque plateaued and extension decreased linearly. Thus, when the plectonemic DNA was held under a constant force, a constant torque condition

could be achieved. When DNA was (–) supercoiled when held at a force ≥ 0.5 pN, DNA began to melt before buckling. As shown, the buckling torque was symmetric for (+) and (–) DNA supercoiling until the applied torque reached –10.5 pN•nm at ~ 0.5 pN where DNA instead underwent a melting transition. Beyond this force (> 0.5 pN), torque during (+) supercoiling continued to increase with increasing force while torque during (–) supercoiling plateaued with increasing force. Each dashed vertical line indicates the onset of a bucking or melting transition.

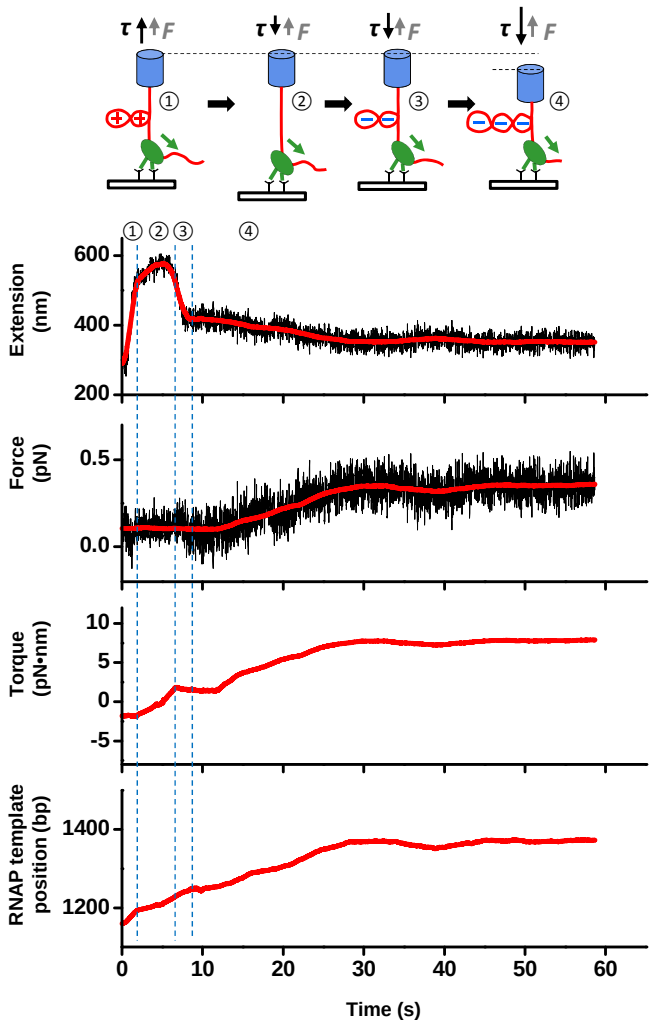

Figure S4. A representative set of data for upstream stall torque measurements.

After introducing 1 mM NTPs to the experimental chamber, the force on the DNA was clamped at a low force of 0.15 pN by modulation of the coverslip height, while DNA was mechanically overwound until a (+) plectoneme was formed behind the RNAP. Subsequent translocation of RNAP was evidenced by a sharp increase in DNA extension (①), until the pre-established (+) plectoneme was totally neutralized. The translocation

of RNAP on non-buckled DNA only caused DNA extension to change moderately (②). Further translocation of the RNAP resulted in (–) plectoneme formation, leading to a sharp decrease of the DNA extension (③). The force clamp was then turned off and the coverslip position was kept fixed (④). As the RNAP continued to translocate, the quartz cylinder was pulled towards the RNAP, and thus away from the trap center, resulting in a slight increase in force and a corresponding increase in torque (Fig. S3), until RNAP was finally stalled (< 1 bp/s for 20-50 s). Extension data were filtered to 40 Hz (black) and 0.8 Hz (red). Force data were filtered to 40 Hz (black) and 0.13 Hz (red).

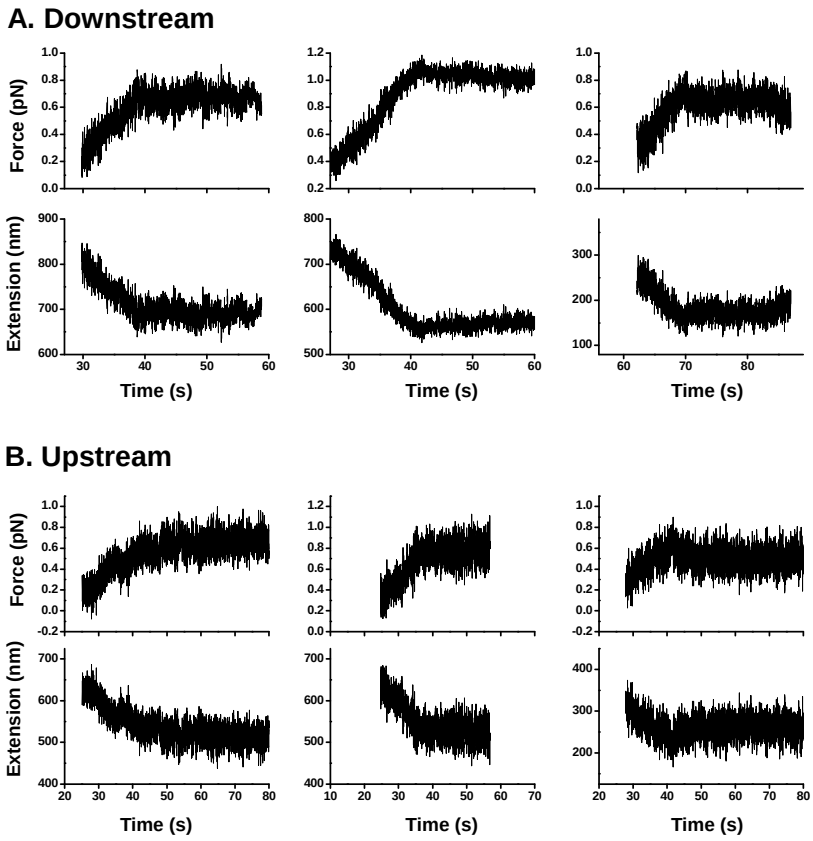

Figure S5. More examples of stalling traces. (**A**) Force and extension of the downstream (+) supercoiled DNA. (**B**) Force and extension of the upstream (–) supercoiled DNA.

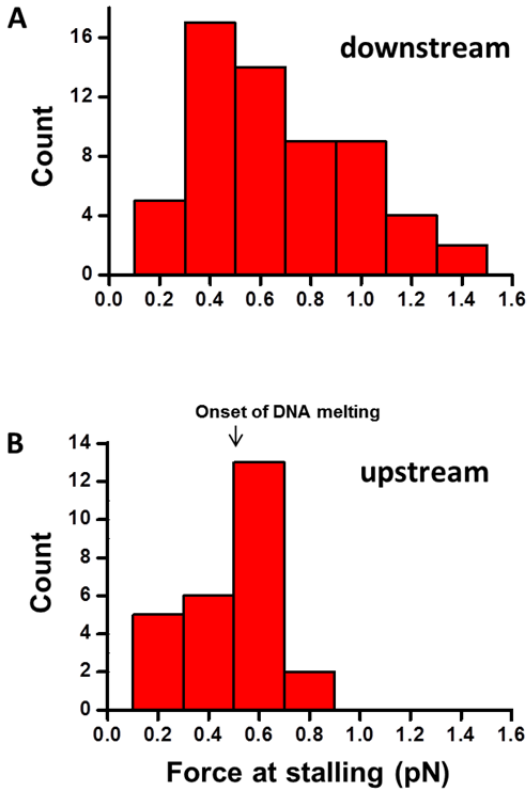

Figure S6. Distributions of force in DNA when RNAP was stalled under torsion. (**A**) RNAP polymerase was stalled against (+) plectonemic DNA held under force. The corresponding stall torque is shown in Fig. 2A. (**B**) RNAP polymerase was stalled against (–) plectonemic DNA or melted DNA held under force. The corresponding stall torque is shown in Fig. 2B.

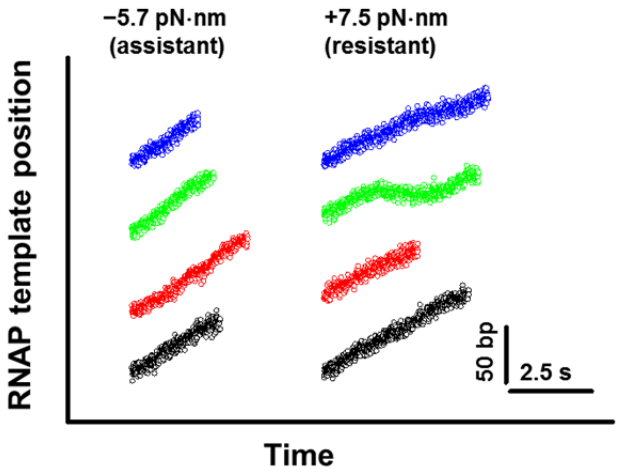

Figure S7. More example traces of transcription under a constant torque. Both axes were arbitrarily shifted for ease of comparison. Transcription was measured under either a resisting torque of – 5.7 pN·nm or an assisting torque of + 7.5 pN·nm.

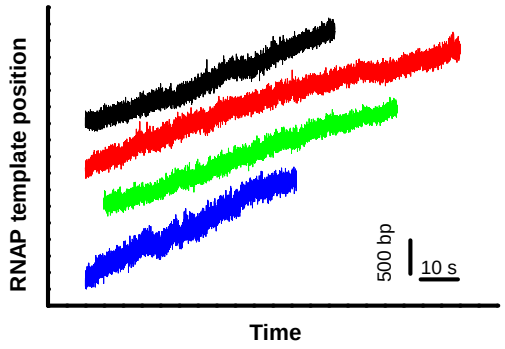

Figure S8. Example traces for transcription under zero torque.

Measurements were conducted with the "downstream" template under 0.3 pN resisting force. Traces are arbitrarily shifted in both axes for clarity.

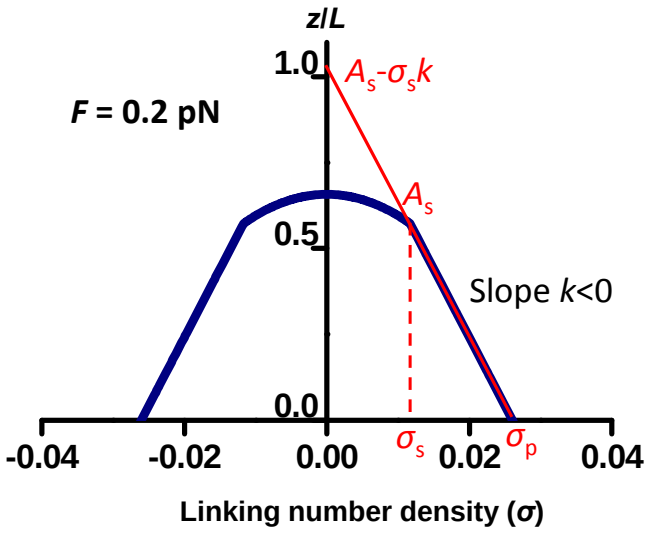

Figure S9. A cartoon illustrating the relation between the normalized extension and linking number density.

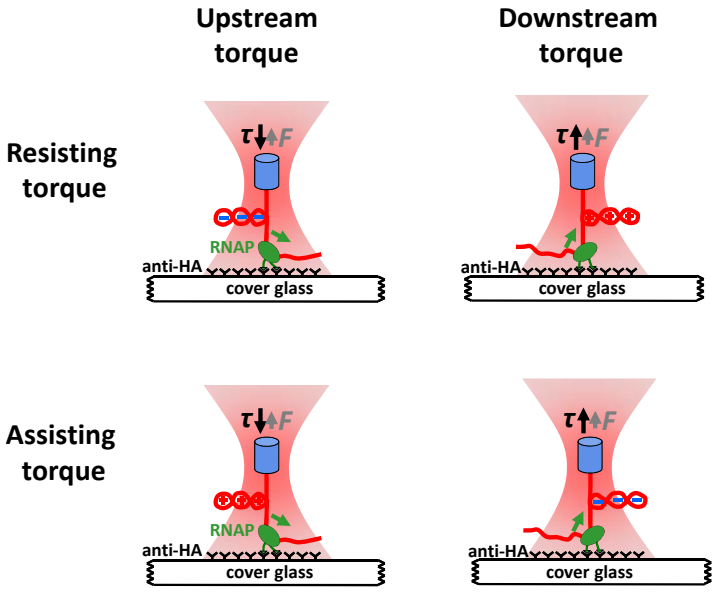

Figure S10. Possible experimental configurations to study transcription under torque using an AOT. Torque can be exerted either upstream or downstream of the RNAP, and can be either assisting or resisting transcription.

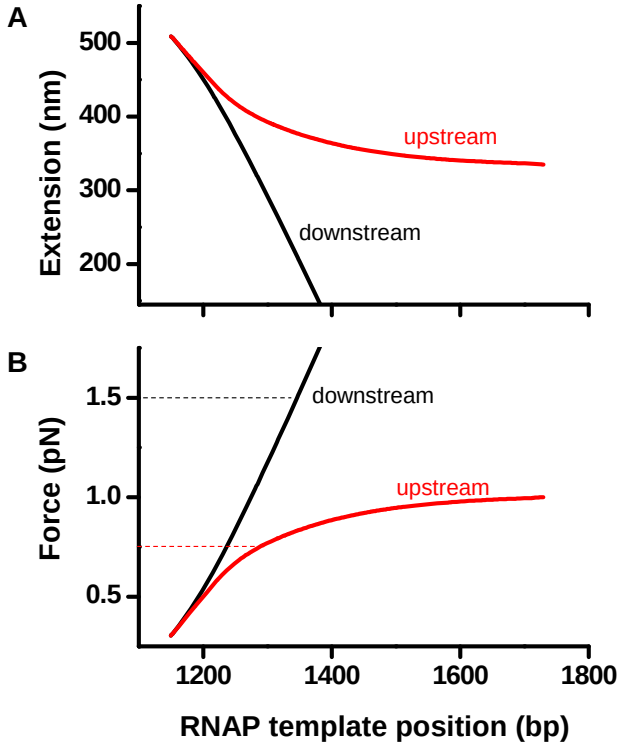

Figure S11. Simulated extension **(A)** and force **(B)** in response to transcription as RNAP approaches a stall.

The simulations were performed for both downstream and upstream stalling during step 4. At the beginning of step 4, RNAP template position was assumed to be 1150 bp and 8 turns were stored in the DNA to allow it to buckle. Transcription results in extension shortening and force increase. For the downstream case, there is a rather linear relation between force and RNAP template position. For the upstream case, the force becomes less sensitive to RNAP translocation once the DNA starts melting. However, the force still holds a rather good sensitivity for $F \leq 0.75$ pN (the maximum upstream force in

DNA when RNAP was stalled). The dashed lines indicate the maximum measured force at a stall for downstream (black) and upstream (red) experiments.

Movie S1. Direct visualization of transcription generated DNA rotation in real time.

The downstream template was used for this demonstration. The quartz cylinder was not trapped and its motion was only constrained by its attachment to the DNA (see cartoon below). In the absence of NTPs, the tethered cylinder randomly moved around the coverslip-bound RNAP. After the addition of NTPs, the cylinder rotated clockwise at about 0.6 Hz. The detected direction of rotation, given the imaging optics used, showed that RNAP rotated in a right-handed fashion as it translocated along the DNA, consistent with its tracking of the groove of the right-handed DNA. The rotation speed corresponded to about 7 bp/s. This reduced speed was due to the viscous drag torque exerted on the cylinder and pausing during RNAP translocation.

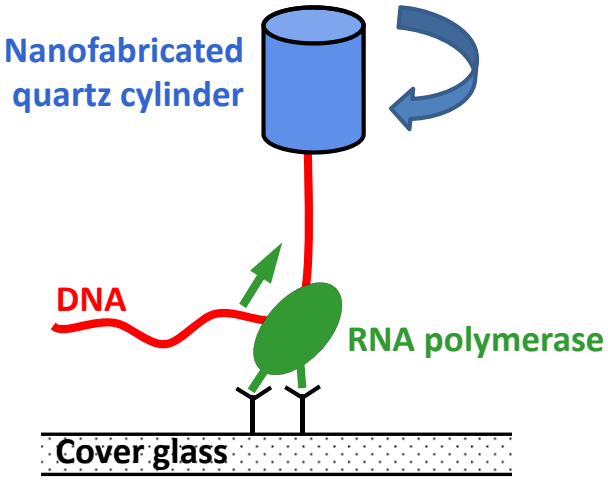

References

1. L. F. Liu, J. C. Wang, *Proc. Natl Acad. Sci. USA* **84**, 7024 (1987).
2. A. Travers, G. Muskhelishvili, *Nat. Rev. Micro.* **3**, 157 (2005).
3. F. Kouzine, J. Liu, S. Sanford, H.-J. Chung, D. Levens, *Nat. Struct. Mol. Biol.* **11**, 1092 (2004).
4. F. Kouzine, S. Sanford, Z. Elisha-Feil, D. Levens, *Nat. Struct. Mol. Biol.* **15**, 146 (2008).
5. K. Matsumoto, S. Hirose, *J. Cell Sci.* **117**, 3797 (2004).
6. H.-Y. Wu, S. Shyy, J. C. Wang, L. F. Liu, *Cell* **53**, 433 (1988).
7. A. La Porta, M. D. Wang, *Phys. Rev. Lett.* **92**, 190801 (2004).
8. C. Deufel, S. Forth, C. R. Simmons, S. Dejgosha, M. D. Wang, *Nat. Meth.* **4**, 223 (2007).
9. S. Forth *et al.*, *Phys. Rev. Lett.* **100**, 148301 (2008).
10. M. Y. Sheinin, S. Forth, J. F. Marko, M. D. Wang, *Phys. Rev. Lett.* **107**, 108102 (2011).
11. Materials and methods are available as supplementary material on *Science* Online.
12. Y. Harada *et al.*, *Nature* **409**, 113 (2001).
13. A. Revyakin, R. H. Ebright, T. R. Strick, *Proc. Natl Acad. Sci. USA* **101**, 4776 (2004).
14. A. Revyakin, C. Liu, R. H. Ebright, T. R. Strick, *Science* **314**, 1139 (2006).
15. L. Bai, A. Shundrovsky, M. D. Wang, *J. Mol. Biol.* **344**, 335 (2004).
16. L. Bai, R. M. Fulbright, M. D. Wang, *Phys. Rev. Lett.* **98**, 068103 (2007).
17. L. Bai, M. D. Wang, *J. Stat. Mech.* **2010**, P12007 (2010).

18. D. M. J. Lilley, C. F. Higgins, *Mol. Microbiol.* **5**, 779 (1991).

19. D. Kowalski, M. J. Eddy, *EMBO J.* **8**, 4335 (1989).

20. N. Komissarova, M. Kashlev, *Proc. Natl Acad. Sci. USA* **94**, 1755 (1997).

21. J. W. Shaevitz, E. A. Abbondanzieri, R. Landick, S. M. Block, *Nature* **426**, 684 (2003).

22. E. A. Galburt *et al.*, *Nature* **446**, 820 (2007).

23. D. Dutta, K. Shatalin, V. Epshtein, Max E. Gottesman, E. Nudler, *Cell* **146**, 533 (2011).

24. T. R. Strick, V. Croquette, D. Bensimon, *Nature* **404**, 901 (2000).

25. D. A. Koster, V. Croquette, C. Dekker, S. Shuman, N. H. Dekker, *Nature* **434**, 671 (2005).

26. J. Gore *et al.*, *Nature* **439**, 100 (2006).

27. V. Levchenko, B. Jackson, V. Jackson, *Biochemistry* **44**, 5357 (2005).

28. C. Lavelle, *Biochimie* **89**, 516 (2007).

29. K. Adelman *et al.*, *Proc. Natl Acad. Sci. USA* **99**, 13538 (2002).

30. S. Forth, M. Y. Sheinin, J. Inman, M. D. Wang, *Annu. Rev. Biophys.* **42**, 583 (2013).

31. Z. Huang, F. Pedaci, M. van Oene, M. J. Wiggin, N. H. Dekker, *ACS Nano* **5**, 1418 (2011).

32. A. I. Bishop, T. A. Nieminen, N. R. Heckenberg, H. Rubinsztein-Dunlop, *Phys. Rev. A* **68**, 033802 (2003).

33. J. Jin *et al.*, *Nat Struct Mol Biol* **17**, 745 (2010).

34. A. Shundrovsky, T. J. Santangelo, J. W. Roberts, M. D. Wang, *Biophys. J.* **87**, 3945 (2004).

35. C. E. Aitken, R. A. Marshall, J. D. Puglisi, *Biophys. J.* **94**, 1826 (2008).

36. E. J. G. Peterman, F. Gittes, C. F. Schmidt, *Biophys. J.* **84**, 1308 (2003).

37. J. F. Marko, *Phys. Rev. E* **76**, 021926 (2007).

38. T. R. Strick, J.-F. Allemand, D. Bensimon, A. Bensimon, V. Croquette, *Science* **271**, 1835 (1996).

39. A. Sarkar, J.-F. Léger, D. Chatenay, J. F. Marko, *Phys. Rev. E* **63**, 051903 (2001).

40. Z. Bryant *et al.*, *Nature* **424**, 338 (2003).

41. A. Celedon *et al.*, *Nano Lett.* **9**, 1720 (2009).

42. J. Lipfert, J. W. J. Kerssemakers, T. Jager, N. H. Dekker, *Nat Meth* **7**, 977 (2010).

43. F. C. Oberstrass, L. E. Fernandes, Z. Bryant, *Proc. Natl Acad. Sci. USA* **109**, 6106 (2012).

44. F. C. Oberstrass, L. E. Fernandes, P. Lebel, Z. Bryant, *Physical Review Letters* **110**, 178103 (2013).

45. D. Salerno *et al.*, *Phys. Rev. Lett.* **109**, 118303 (2012).

46. A. Tempestini *et al.*, *Nucl. Acids Res.*, (2012).

47. F. Mosconi, J. F. Allemand, D. Bensimon, V. Croquette, *Phys. Rev. Lett.* **102**, 078301 (2009).

48. P. R. Cook, *Science* **284**, 1790 (1999).

49. P. Nelson, *Proc. Natl Acad. Sci. USA* **96**, 14342 (1999).

50. K. C. Neuman, E. A. Abbondanzieri, R. Landick, J. Gelles, S. M. Block, *Cell* **115**, 437 (2003).

51. M. D. Wang *et al.*, *Science* **282**, 902 (1998).